Influence of Slag Viscosity on Copper Matte Entrainment Volume by a Rising Bubble Through Immiscible Liquids Interface

Xiangfeng Cheng, Mao Chen, Fuming Zhang, Gele Qing, and Jianlong Wu

Abstract In the settlement zone of the copper smelting furnace, SO_2 bubbles will be generated due to the insufficient oxidization of copper matte concentrate by injected oxygen-rich air in the reaction zone, entailing mass transfer in the liquid–liquid system by a rising bubble penetrating through the liquid–liquid interface. Different operating conditions between the bottom blown furnace and side blown furnace lead to different slag and matte viscosity. To investigate the copper smelting slag viscosity effect on the matte entrainment volume, cold model experiments using high-speed imaging techniques and high-temperature experiments were carried out. Results show that the lower liquid entrainment volume increases with the decreasing upper liquid viscosity and increasing bubble size. Higher slag viscosity and more SO_2 bubbles generated in the side blown furnace probably deteriorate the matte entrainment in the slag phase, while matte viscosity exerts slight influences due to the stable viscosity variation.

Keywords Copper smelting · SO_2 bubbles · Slag viscosity · Matte entrainment

X. Cheng · G. Qing · J. Wu
Shougang Research Institute of Technology, Beijing 100043, China

Beijing Key Laboratory of Green Recyclable Process for Iron & Steel Production Technology, Beijing 100043, China

M. Chen (✉)
State Key Laboratory of Vanadium and Titanium Resources Comprehensive Utilization, Panzhihua 617000, Sichuan, China
e-mail: ptchenmao@163.com

F. Zhang
Shougang Group, Beijing 100041, China

Introduction

The demand for copper has been increasing for the last decades with an increase of exploitation quantity, while a significant loss of copper in the slags happens in the smelting process simultaneously. Generally, the copper loss can be classified into physical entrainment, e.g., entrained matte droplets and chemical entrainment, e.g., Cu^+ ions with O^{2-} or S^{2-} ions. Several sources of entrained matte in slags are reported in the previous studies [1, 2]. The slag chemistry studies of bottom blown furnace (BBF) and side blown furnace, e.g., Teniente Converter (TC) indicate that the majority of the copper losses to the slag are the mechanically entrapped matte droplets.

In the relatively static environment of settlement zone in bath smelting furnace, numerous SO_2 gas bubbles are generated from the further oxidization of copper matte in the matte phase, leading to a significant mass transfer when penetrating matte-slag interface, as shown in Eq. 1.

$$CuFeS_2(s) + O_2(g) + SiO_2(s) \rightarrow (Cu, Fe, S)(l) + FeO - SiO_2(l) + SO_2(g) \quad (1)$$
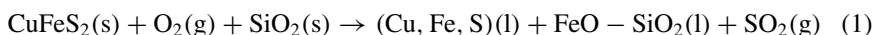
Numerous SO_2 bubbles penetration process through the immiscible matte-slag interface is expected to cause matte entrainment in the slag phase. The matte and bubble size distributions in industrial slag samples in bottom blown furnace and Teniente Converter have been analyzed, while the copper losses in two furnaces are different with about 3% in bottom blown furnace and up to 12% in the Teniente Converter [2, 3] (Fig. 1).

Single bubble rising behaviours through the liquid–liquid interface are highly dynamic processes applied in numerous industrial applications, e.g., metallurgical processes, nuclear reactor safety, etc. [2, 4–8]. Gas bubbles rising across a liquid–liquid interface could carry a surface coating of the lower liquid into the upper phase and scatter small droplets into the slag phase. The film stability was described through
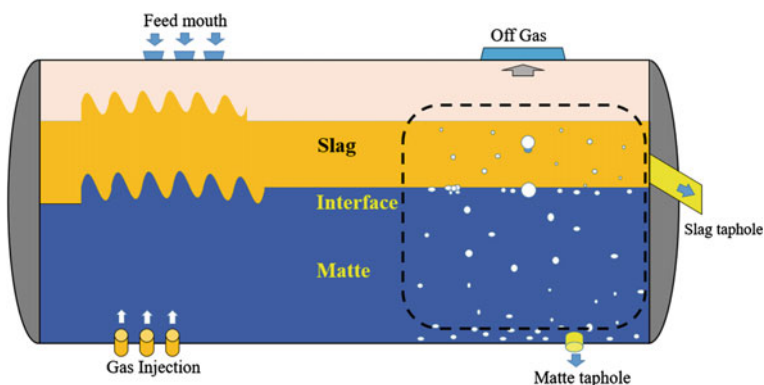

Fig. 1 Rising bubbles generated in the settlement zone of the smelting furnace

floatation coefficient and spreading coefficient by considering the interfacial energies of the bottom blown furnace and side blown furnace (e.g., Teniente Converter (TC)) [1]. The settlement time of matte droplets entrained in the slag phase was estimated, and results showed that the majority of copper matte droplets observed in slags were difficult to settle down during periodic discharging time [2].

Many experimental and numerical studies have been carried out on bubble passage through the immiscible liquids interface [4, 9–11]. The passage of bubble rise in fluids and at the interface was followed, and the dynamic behaviour of the interface was investigated by the bubble's position and the corresponding retention time at the interface. Moreover, many researchers have reported the film enveloping the bubble or the column between the bubble and the lower interface caused by rising bubbles at the interface in several combinations of liquid–liquid systems [12].

The viscosity of smelting slags is an important process variable to reflect the flow behaviours in most pyrometallurgical smelting operations and has a strong influence on rates of mixing of mass transfer, metal and slag separation, etc. The copper matte is a combination of copper sulphide, a small amount of iron sulphide and some heavy metals, of which copper sulphide makes up 80–95%. The temperature and composition of slags have great effects on slag viscosity [13]. Due to the limited varying range of matte viscosity, the temperature has little impact on the dynamic viscosity of the pure compounds Cu_2S, FeS, and also the pseudo-binary systems of FeS–Cu_2S. The dynamic viscosity of melts in the Cu_2S–FeS system is less affected by temperature, varying slightly from 0.002 to 0.004 Pa s. Thus, the operating temperature in the smelting furnace mainly depends on the molten slag requirement. Besides, the matte grade in the bottom blown furnace is similar to that in the Teniente Converter at approximately more than 70%, while the oxygen enrichment is far higher in bottom blown smelting furnace at 72–73% than in side blown smelting furnace typically at 35–42%.

This paper aims to explore the copper matte and smelting slag viscosity effects on the copper matte entrainment volume in the slags with cold model experiments and high-temperature validation experiments.

Experimental

Experimental Setup

Copper matte transport process from the matte phase to upper slag phase through immiscible matte-slag interface at high temperatures is difficult to be observed directly. To simulate and visualize the whole transporting process at the interface and quantify the lower liquid entrainment volume by rising bubbles when passing through the interface, cold model experimental setup was used to capture bubble penetration behaviours through the liquid–liquid interface, as shown in Fig. 2a. Cold model experimental setup consisted of a transparent glass container (80 mm * 80 mm * 600
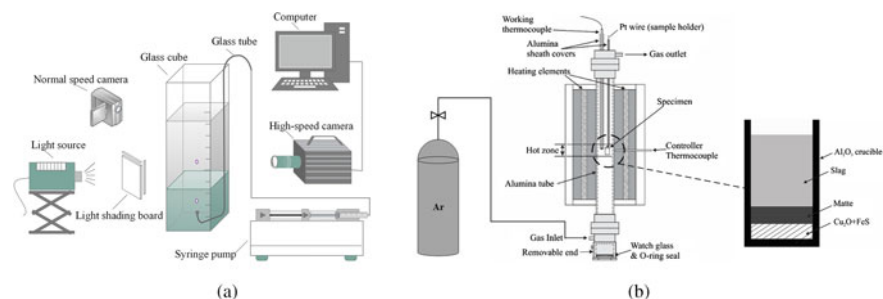
Fig. 2 Schematic diagram of an experimental device in **a** cold model experiments and **b** high-temperature experiments

mm), and a high-speed camera to capture the bubble penetration behaviours and measure the lower liquid entrainment volume at 500 fps. A light source (XGY-II, Zhejiang Xinguangyang Lighting Co., Ltd.) at the opposite direction of the high-speed camera was used to provide dispersed light through a light shading board to illuminate liquids in the glass cube. Air was fed from a syringe pushed by an infusion pump (Kd Scientific 780100, ALT) to control the air flow rate precisely.

High-temperature experiments in the laboratory were carried out to verify the attachment between matte droplets and SO_2 bubbles and further explore the slag viscosity influence on matte entrainment. Scanning Electron Microscope (SEM) was used to determine the microstructures of the quenched laboratory slags. The schematic diagram of the furnace inner structure and experimental setup are displayed in Fig. 2b. High-temperature experiments were conducted in a vertical tube furnace using alumina crucibles (inner dimensions: 2 cm diameter, 5 cm high). Samples were prepared in three layers (Fig. 2b): a slag layer at the top, a matte layer in the middle, and a mixture of Cu_2O and FeS at the bottom. The bottom layer with Cu_2O and FeS mixture is to generate SO_2 bubbles in the melts.

Materials

In the cold model experiments, solutions of glycerol with different concentrations in the water and silicone oils with different viscosities were used to investigate the lower liquid and upper liquid viscosity effects on the lower liquid entrainment volume, respectively, as given in Table 1.

It should be noted that upper liquid entrainment volume was defined as the total lower liquid droplets volume transporting into upper liquid by a rising gas bubble.

The synthetic slags were also used to observe the slag viscosity effects on bubble penetration behaviours at the matte-slag interface. The slag physical properties are given in Table 2.

Table 1 Physical properties of liquid–liquid combination systems

Lower phase				Upper phase			
Material	Viscosity (cP)	Density (g/cm^3)	Surface tension (mN/m)	Material	Viscosity (cP)	Density (g/cm^3)	Surface tension (mN/m)
Glycerol 80%	60.1	1.21	48.06	10 cP silicone	10	930	20.1
Glycerol 70%	22.5	1.19	48.26	50 cP silicone	50	959	20.7
Glycerol 60%	10.8	1.16	48.11	200 cP silicone	200	970	21.1
Glycerol 40%	3.72	1.10	48.66	500 cP silicone	500	970	21.1

Table 2 Physical properties of synthetic slag samples in high-temperature experiments

Samples	Synthetic slags (wt%)				Melting point (°C)	Viscosity (Pa s)
	CaO (g)	Fe (g)	Fe$_2$O$_3$ (g)	SiO$_2$ (g)		
No. I	3.4888	3.9801	10.3379	0	1141	0.022
No. II	2.6168	2.2389	5.815	6.9781	1117	0.273

In Experiment No. I, approximately 20% CaO and 80% FeO were mixed to form slags with lower viscosity, while more SiO$_2$ (40%) and less FeO (45%) were mixed with CaO to generate slag with higher viscosity in Experiment No. II. The chemicals Cu$_2$O (≥99.99%) and FeS (≥99.9%; both Sigma-Aldrich, USA) were mixed to generate SO$_2$ bubbles at the bottom of the Al$_2$O$_3$ crucible. The pelletized Cu$_2$O and FeS mixture was placed at the bottom of the crucible to generate SO$_2$ bubbles to simulate the bubble transportation process in the smelting furnace.

Experimental Procedures

Immiscible glycerol solution and silicone oil systems in the cold model experiments were used to simulate the matte and slag systems in the copper smelting furnace. In different glycerol-silicone oil systems, air was fed by a syringe pump at different injection flow rates and glass nozzle sizes to control bubble size. The bubble size could be controlled through some specially made glasses which are replaceable in the notch of gas injection tube. Seven specially made glass nozzles (inner diameters: 0.5 mm, 3 mm, 4 mm, 5 mm, 6 mm, 7 mm, 9 mm) were used to generate bubbles varying from 2 to 10 mm in diameter. All experiments were carried out at 25 °C. The bubble size and lower liquid entrainment volume in the upper phase can be measured by Image J with high-speed imaging techniques.

High-temperature experiments were conducted in a vertical tube furnace in the Ar atmosphere (99.999%). The specimen was heated to 600 °C at 15 °C/min and placed in the furnace at 600 °C to dry for 30 min firstly. Then, samples were heated to 900 °C at 5 °C/min. Two three-layer samples were heated to 1200 °C. The specimen was kept at 1200 °C for 10 min to release as many bubbles as possible, and then lowered rapidly to the cold end of the furnace. The crucible was fast-quenched by the high-purity Ar gas.

Results and Discussion

Bubble size plays a significant role in the distinct bubble penetration regimes through immiscible liquids interface. Small bubbles, generally 2.5–4.5 mm in diameter, referred to those which cannot penetrate the interface directly due to the interfacial resistance at the first impact. Large gas bubble, generally larger than 4.5 mm in diameter, can penetrate liquid–liquid interface directly with a long liquid column due to the large momentum. However, lower liquid column dragged by rising gas bubble in the upper phase tend to detach from the bubble before it ruptures into small droplets. The threshold for small and large bubbles depends on the fluids physical properties in different immiscible liquid–liquid systems [1, 4].

Lower Liquid Entrainment Volume by a Small Rising Gas Bubble

Bubble passage through two immiscible liquids interface shows a strong correlation with bubble size and fluids physical properties. Fine bubbles in the millimeter or submillimeter range tend to induce a barely perceptible lower liquid film to surround a gas bubble or scattered fine lower liquid droplets to be attached to the bubble surfaces [2]. However, for small bubbles with diameters more than 2.5 mm shown in Fig. 3a–d, a stable attachment between a thick lower liquid layer and a rising gas bubble tends to be formed in silicone oils at different viscosities although it may not inevitably happen in different immiscible liquid–liquid systems, which can lead to the detachment height as high as 500 mm. Moreover, it was found that a long thin column or tail tends to be formed in the 10 cP silicone oil as shown in Fig. 3a and caused more scattered lower liquid droplets when it ruptured behind the rising bubble. The reason for this type of behaviour can be attributed to the larger silicone oil viscosity as an equivalent bubble requires only a smaller buoyancy force to overcome the viscous force from the silicone oil to penetrate the interface and enable bubble passage by greater kinetic energy. Thus, for bubbles in Fig. 3d, silicone oil with a viscosity of 500 cP will make it difficult for small bubbles to pass through the interface and possess sufficient momentum to induce the long tail. Thus, a larger
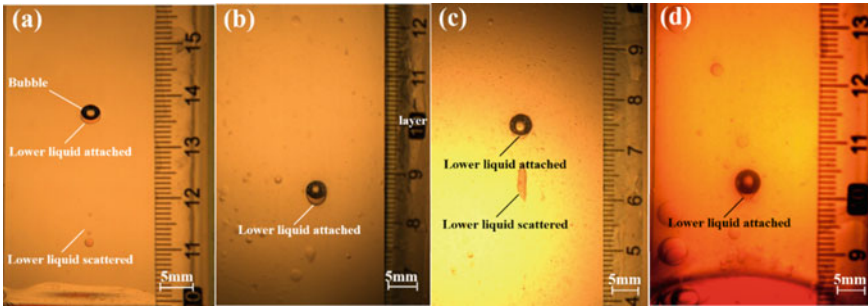
Fig. 3 Medium bubble and lower liquid attachment at different upper liquid viscosities of **a** 10 cP, **b** 50 cP, **c** 200 cP, and **d** 500 cP

upper liquid viscosity will inhibit the total entrainment volume of lower liquid in the upper liquid phase.

Lower Liquid Entrainment Volume by a Larger Rising Gas Bubble

As the bubble size increases, flow regimes during the passage of a rising bubble through a liquid–liquid interface will be different. Figure 4a–d shows the bubbles with diameters of 6.3 mm, 6.1 mm, 6.0 mm, and 5.9 mm in 10 cP, 50 cP, 200 cP, and 500 cP silicone oil, respectively. In Fig. 4a, the bubble shows an irregular shape and experiences severe deformation due to the smaller silicone oil viscosity at 50 cP. However, with the increase of silicone oil viscosity in Fig. 4b–d, the bubble present regular shapes, i.e., a spherical cap, ellipsoidal, and nearly spherical shape, respectively. In Fig. 4a and b, a large lower water droplet from the ruptured water column was observed to rise behind a rising bubble, which size was comparable to the rising bubble. In Fig. 4c and d, a long tail tends to be formed behind the rising bubble due to the larger upper liquid viscosity, while an obvious lower liquid layer was attached at the rear of the bubble in Fig. 4d. This is probably because the larger silicone oil viscosity favors the stability of the bubble shape and therefore a more stable attachment of the lower liquid layer to the bubble surface.

Attachment Between SO$_2$ Bubble and Matte in Copper Smelting Slags

To investigate the slag viscosity effect on the attachment volume of copper matte by the numbers of SO$_2$ bubbles in smelting slags, high-temperature experiments were carried out. Figure 5 shows the attachment between SO$_2$ bubbles and copper matte
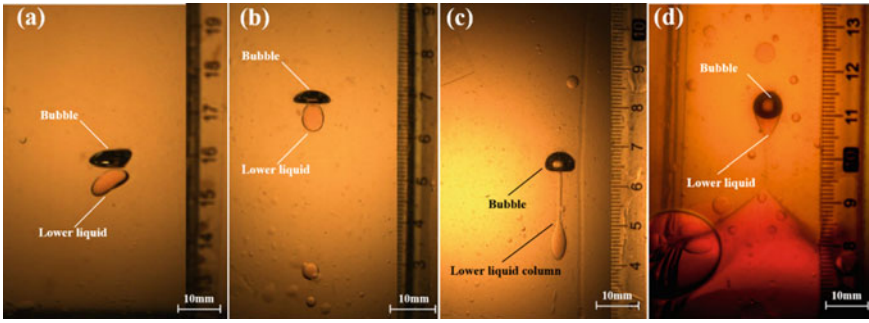
Fig. 4 Large bubble and lower liquid attachment at different upper liquid viscosities **a** 10 cP, **b** 50 cP, **c** 200 cP, and **d** 500 cP

in different smelting slags with slag viscosity of 0.022 Pa s in Fig. 5a and 0.273 Pa s in Fig. 5b. From SEM photographs, it was found that SO_2 bubbles in the smelting slags in both Fig. 5a and b ranged from 50 to 500 µm. A larger number of SO_2 bubbles were observed to distribute in the smelting slags in Fig. 5a compared with the number of bubbles in Fig. 5b, while the average bubble size is comparatively smaller than that in Fig. 5b. This is probably because higher slag viscosity inhibits the small bubble penetration through the matte-slag interface, leading to a smaller number of but larger SO_2 bubbles in the slags. It should be noted that the volume ratio between matte droplets and gas bubbles in Fig. 5a presents a larger value than that in Fig. 5b, meaning more matte droplets tend to be carried into smelting slags with lower viscosities for SO_2 bubbles at an equivalent size. Therefore, the ascending slag viscosity can significantly increase the matte entrainment volume for a rising SO_2 bubble through the immiscible matte-slag interface, which was in good agreement with the results shown in cold model experiments.
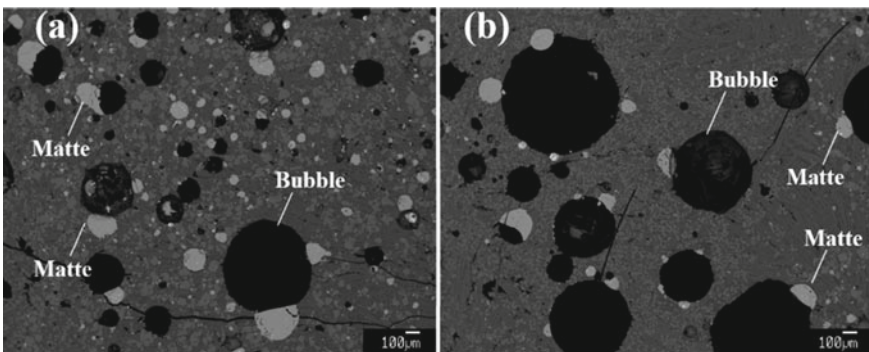

Fig. 5 SO_2 bubble and matte attachment in slags at different viscosities: **a** slag viscosity: 0.022 Pa s; **b** slag viscosity: 0.273 Pa s

Discussion

The lower liquid film thickness was derived by the total lower liquid entrainment volume and bubble size, which assumes the lower liquid droplets spread on the bubble surfaces evenly.

Figure 6 shows the effects of silicone oil viscosity (10 cP, 50 cP, 200 cP, 500 cP) effects on water entrainment volume for different sized bubbles. The interfacial tension between water and silicone oils was controlled at approximately 50 mN/m. The entrained water thickness on the bubble surface shows a good correlation with the bubble size assuming the water droplets were evenly spreading on the spherical bubble surface. The lower liquid layer thickness increases with the increase of bubble size and decrease of silicone oil viscosities from 500 to 10 cP. Besides, the difference of water film thickness becomes more significant with the increase of the bubble size.

Figure 7 shows the lower liquid viscosity effects on lower liquid thickness at a rising bubble. It can be found that with the increasing lower liquid viscosity, the lower liquid thickness on the bubble surfaces decreases. However, the lower liquid thickness showed not much difference when the lower liquid viscosity reached above 22.5 cP.
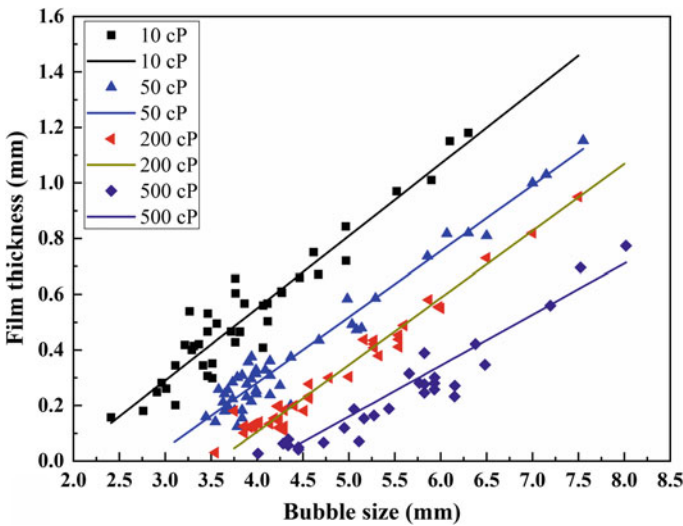

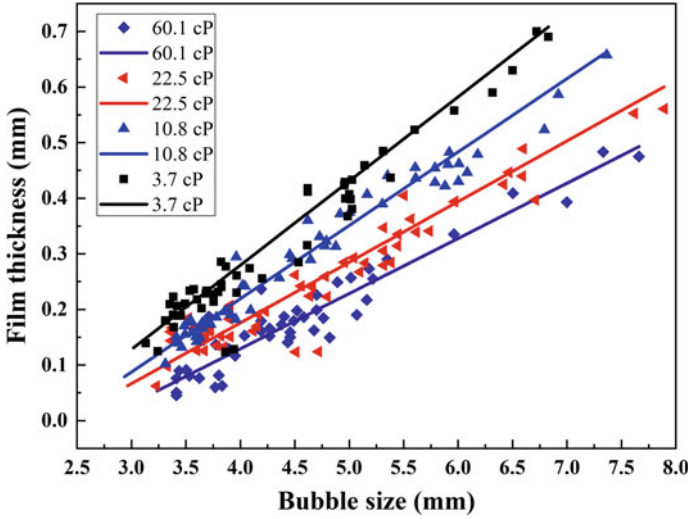**Fig. 6** Upper liquid viscosity effects on lower liquid thickness at a rising bubble

Fig. 7 Lower liquid viscosity effects on lower liquid thickness at a rising bubble

Conclusions

Copper matte and smelting slags viscosity effect on the matte entrainment volume has been carried out. Experimental results show that the water entrainment volume increases with decreasing silicone viscosity and increasing bubble size. High-temperature experimental results show a good agreement with the cold model experiments that the smelting slag with higher viscosity can inhibit the matte entrainment in the slags in terms of the number of SO_2 bubbles and matte entrainment volume.

From the perspective of industrial application, lower oxygen enrichment in the side blown furnace (35–42%) than that in bottom blown furnace (72–73%) facilitates the generation of more SO_2 bubbles ranging from millimeters to microns in the settlement zone of the smelting furnace, thus leading to more copper matte entrainment in the slags. Besides, the dynamic viscosity of matte, i.e., Cu_2S–FeS system, is less affected by temperature, varying slightly from 0.002 to 0.004 Pa s. However, the slag viscosity μ_{slag} in Teniente Converter (0.124 Pa s) is smaller than that in a bottom blown furnace (0.180 Pa s) due to the higher temperature (TC: 1250 °C; BBF: 1170 °C) and lower SiO_2, Fe_3O_4 contents. The lower slag viscosity contributes to the copper matte entrainment in the side blown furnace.

References

1. Greene GA, Chen JC, Conlin MT (1991) Bubble induced entrainment between stratified liquid layers. Int J Heat Mass Tran 34(1):149–157
2. Cheng XF, Cui ZX, Contreras L, Chen M, Nguyen VA, Zhao BJ (2019) Matte entrainment by SO_2 bubbles in copper smelting slag. JOM 71(5):1897–1903
3. Cheng, XF, Contreras L, Chen M et al (2017) Introduction of matte droplets in copper smelting slag. Paper presented at the 8th international symposium on high-temperature metallurgical processing, TMS 2017
4. Emery TS, Raghupathi AP, Kandlikar GS (2018) Flow regimes and transition criteria during passage of bubbles through a liquid-liquid interface. Langmuir 34(23):6766–6776
5. Shi WB, Yang XG, Sommerfeld M et al (2019) Modelling of mass transfer for gas-liquid two-phase flow in bubble column reactor with a bubble breakage model considering bubble-induced turbulence. Chem Eng J 371:470–485
6. Kapusta JPT (2017) Submerged gas jet penetration: a study of bubbling versus jetting and side versus bottom blowing in copper bath smelting. JOM 69(6):970–979
7. Saito T, Toriu M (2015) Effects of a bubble and the surrounding liquid motions on the instantaneous mass transfer across the gas–liquid interface. Chem Eng J 265:164–175
8. Singh KK, Bart HJ (2019) Passage of a bubble through the interface between a shear-thinning heavier liquid and a Newtonian lighter liquid. Chem Eng Commun, 1–18
9. Mao N, Teng S, Mulbah C (2020) Formation and detachment of the enclosing water film as a bubble passes through the water-oil interface. Colloids Surf A Physicochem Eng Asp 586:124236
10. Singh KK, Gebauer F, Bart HJ (2017) Bouncing of a bubble at a liquid–liquid interface. AIChE J 63(7):3150–3157
11. Singh KK, Bart HJ (2015) Passage of a single bubble through a liquid–liquid interface. Ind Eng Chem Res 54(38):9478–9493
12. Farhadi J, Sattari A, Hanafizadeh P (2022) Passage of a rising bubble through a liquid-liquid interface: a flow map for different regimes. Can J Chem Eng 100(2):375–390
13. Chen M, Raghunath S, Zhao B (2014) Viscosity measurements of SiO_2-"FeO"-MgO system in equilibrium with metallic Fe. Metall Mater Trans B 45(1):58–65